Title: Pegylation of biodegradable dextran nanogels for siRNA delivery

Authors: Naeye B., Raemdonck K., Remaut K., Sproat B., Demeester J., De Smedt S.C.

In: European Journal of Pharmaceutical Sciences, 40(4), 342-351 (2008)

Optional: link to the article

Submitter : Pharm. Broes Naeye
Laboratory of General Biochemistry and Physical Pharmacy
Ghent University
Harelbekestraat 72
9000 Ghent
BELGIUM
Tel: +32 9 264 80 74
Fax: +32 9 264 81 89
e-mail: Broes.Naeye@UGent.be

Other authors: Dr. Koen Raemdonck, Dr. Katrien Remaut, Dr. Brian Sproat, Prof. Dr. Joseph Demeester

Corresponding Author: Prof. Dr. Stefaan C. De Smedt
Laboratory of General Biochemistry and Physical Pharmacy
Ghent University
Harelbekestraat 72
9000 Ghent
BELGIUM
Tel: 003292648076
Fax: 003292648189
e-mail: Stefaan.Desmedt@ugent.be

Manuscript type: Article

Manuscript title:
'PEGYLATION OF BIODEGRADABLE DEXTRAN NANOGELS FOR SIRNA DELIVERY'

Significance of the manuscript

Dear Editor,

In this paper we report on various ways to PEGylate dextran nanogels. PEGylation could be a valuable asset for the application of dextran nanogels in vivo as this will probably result in an improved pharmacokinetic profile of these carriers. We have shown that covalent coupling of PEG to nanogels is possible and that this approach is most suited compared to other methods of PEGylation.

We hope that our manuscript will be of interest to your readership,

With kind regards,

Broes Naeye

This manuscript, or its contents in some other form, has not been published previously by any of the authors and is not under consideration for publication in another journal at the time of submission.

Abstract

Delivering intact siRNA into the cytoplasm of targeted cells *in vivo* is considered a major obstacle in the development of clinically applicable RNAi-based therapies. Although dex-HEMA nanogels have been reported to be suitable carriers for siRNA delivery *in vitro,* and are ideally sized (approximately 180 nm) for intravenous delivery to tumors, they likely possess insufficient blood circulation times to enable an adequate extravasation and accumulation in the tumor tissue. PEGylation of these nanogels should not only improve their circulation time but also minimize their aggregation upon intravenous injection. For this reason, a new type of nanogels and three different methods of PEGylating dextran nanogels were evaluated. Covalent PEGylation of the siRNA loaded nanogels using N-hydroxysuccinimidyl polyethylene glycol (NHS-PEG) was shown to be superior to the addition of both polyethylene glycol (PEG) and PEG grafted poly-L-glutamic acid (PGA-PEG). Flow cytometry and confocal microscopy revealed that PEGylated nanogels are still taken up efficiently by Huh-7 human hepatoma cells and A431 human epithelial carcinoma cells and that the process is cell type dependent. Moreover, PEGylated nanogels loaded with siRNA cause significant EGFP knockdown in Huh-7_EGFP cells and are non toxic for the cells.

Keywords: drug-delivery, siRNA, RNA interference, polyethylene glycol, hydrogel

1. Introduction

Since the initial papers introducing RNA interference (RNAi) and the concept of small interfering RNA (siRNA) (Fire et al., 1998, Elbashir et al., 2001), a plethora of publications have already demonstrated the outstanding potential of siRNA technology for performing loss-of-function studies in cultured cells as well as in whole animals. However, recent studies have indicated that the naturally occurring regulatory role of RNAi is proving to be much more complex than initially anticipated and that the exploitation of this mechanism for clinical purposes should be approached with extreme caution. Considerable effort has already been put into the design of highly effective siRNA molecules causing minimal off-target effects (Grimm, 2009). Equally important as the intelligent design of siRNA molecules is however the development of potent nanosized carriers, since efficient delivery of siRNA is considered to be a major bottleneck in the development of clinically applicable siRNA-based drugs (Raemdonck et al., 2008b, Whitehead et al., 2009). Such carriers should not only prevent degradation and rapid clearance of the siRNA upon intravenous injection (Pack et al., 2005, Braasch et al., 2004, Garcia-Chaumont et al., 1999) but should also guide the siRNA to its intended site of action (Takakura et al., 2002, van de Water et al., 2006, Novobrantseva et al., 2008). The circulation time of nanoparticles can regrettably be very short due to their opsonization mediated recognition and removal by the mononuclear phagocytic system. Opsonization is the process by which a foreign organism/particle becomes covered with opsonin proteins stimulating phagocytosis (Figure 1) and the resulting destruction or removal of the organism/particle from the bloodstream.

One widely used method to prevent or slow down opsonization of nanoparticles in blood is the use of shielding groups which can be either adsorbed or grafted onto their surface. Such groups can block the electrostatic and hydrophobic interactions through which opsonins bind to the surface of particles (Owens and Peppas, 2006). PEGylation, which refers to the decoration of a particle surface by the covalently grafting, entrapping, or adsorbing of polyethylene glycol (PEG) chains, is such a technique (Howard et al., 2008). Some authors claim that PEGylation does not really prevent the binding of opsonins but rather changes the opsonization pattern. This theory is supported by the fact that some proteins seem to behave as dysopsonins, suppressing phagocytic uptake (Moghimi and Patel, 1998, Moghimi and Szebeni, 2003). Additionally, PEGylation can also have a beneficial effect on the stability of dispersed nanoparticles as aggregation is a commonly observed problem upon injection or even during preparation and storage of nanogels. A long circulation of drug loaded nanoparticles and the avoidance of aggregation in the bloodstream is especially important when the nanoparticles have to deliver their drug load into tumors (Figure 1). Indeed, nanoparticles should not be taken up too fast by macrophages and should remain sufficiently small to be able to extravasate through the leaky vasculature in the tumor (Maeda et al., 1999, Ogris and Wagner, 2002). Taking into account the increased clearance rate of delivery systems with a hydrodynamic diameter of more than 200 nm (Moghimi et al., 1993) and the majority of solid tumors exhibiting a vascular pore cut-off size of a few hundred nanometers (Hobbs et al., 1998), carriers smaller than 200 nm should have optimal properties. Moghimi et al. showed however that particles smaller than 100 nm are able to extravasate through fenestrae in the endothelium of the liver and the lymph nodes (Moghimi and Bonnemain, 1999, Wisse et al., 2008). Thus, one can speculate that the

optimal size of the drug loaded nanoparticles when targeting tumor tissues should be between 100 and 200 nm.

Recent work from our group showed that cationic dextran hydroxyethyl methacrylate (dex-HEMA; Figure 2) based nanogels are promising carriers for siRNA delivery since (a) they can be loaded efficiently with siRNA, (b) they are taken up by cells *in vitro* and (c) they are able to deliver intact siRNA into the cytosol of cells (Raemdonck et al., 2009b, Van Thienen et al., 2005). Although such dex-HEMA nanogels are also ideally sized for intravenous delivery to tumors (approximately 180 nm), they likely possess insufficient circulation times to enable an adequate extravasation and accumulation in the tumor tissue (Raemdonck et al., 2009a, Raemdonck et al., 2009b). As discussed above, PEGylation of these nanogels should not only improve their circulation time but also minimize their aggregation following intravenous injection. It has been reported that not all PEGylation techniques are equally effective, as some authors have shown that particles with covalently bound PEG chains achieve longer circulation half-lives than similar particles with physically adsorbed PEG (Bazile et al., 1995, Harper et al., 1991). In order to deliver siRNA *in vivo* by means of dex-HEMA nanogels, we aimed to PEGylate cationic dex-HEMA nanogels using various methods described in this article.

2. Materials and Methods

2.1 Preparation of Cationic Dextran Nanogels. Mini-emulsion photopolymerization was used in order to create modifiable dextran nanogels. Briefly, 100 mg of dextran hydroxyethylmethacrylate (dex-HEMA) or dextran methacrylate (dex-MA, Figure 2,

synthesized as described earlier (vanDijkWolthuis et al., 1997)) was dissolved in 20 mM HEPES buffer at pH 7.4 and supplemented with 500 µmol of cationic methacrylate monomers to a final volume of 400 µL. The cationic monomers [2-(methacryloyloxy)ethyl]trimethylammonium chloride (TMAEMA, Figure 2) and 2-aminoethyl methacrylate hydrochloride (AEMA, Figure 2) were added in different ratios to obtain different cationic dextran nanogels. Subsequently, 60 µL of the photoinitiator Irgacure 2959 (1% w/v in HEPES, Ciba Specialty Chemicals) was added to the mixture. This water phase was emulsified in 3.6 mL light mineral oil (Sigma) containing 10% v/v ABIL EM 90 surfactant (Degussa Goldschmidt (Evonik)) through ultrasonication (Branson Tip Sonifier, 30 s, amplitude 20%). After ultrasonication, the emulsion was briefly cooled before UV irradiation (900 s, 365 nm, Bluepoint 2.1 UV source, Hönle UV technology). In order to remove the continuous phase, the dex-HEMA-*co*-AEMA-*co*-TMAEMA (or dex-MA-*co*-AEMA-*co*-TMAEMA) nanogels were first precipitated with 40 mL of acetone and pelleted down by centrifugation (1500 g, 5 min). After discarding the supernatant the nanogels were redispersed three times in a mixture of acetone/hexane (1:1 v/v) followed by centrifugation (1500 g, 5 min) and removal of the supernatant. The resulting pellet was rehydrated in 5 mL distilled water (4°C) and stored at -20°C until lyophilization. A weighed amount of the lyophilizate was dispersed in a known volume of 20 mM HEPES buffer at pH 7.4 when needed.

2.2 Dynamic Light Scattering (DLS). Size and zeta potential of the nanogels were determined by dynamic light scattering (DLS) using a Zetasizer Nano ZS (Malvern, UK), equipped with Dispersion Technology Software (DTS). The samples were equilibrated at 25°C prior to measurement and measurement settings were set to automatic. The degradation of the nanogels was monitored by DLS measurements on a 0.5 mg mL^{-1} nanogel dispersion in 20

mM HEPES buffer pH 7.4 in a low-volume DLS cuvette sealed with parafilm. The dispersion was incubated at 37°C and the intensity of the scattered light was measured every 5 min.

2.3 Synthesis of Polyethylene Glycol grafted Poly-L-Glutamic Acid (PGA-PEG). Poly-L-glutamic acid (450 µmol, MW: 50 – 100 kDa, Sigma) was dissolved in 3.378 mL phosphate buffer (100 mM, pH 7.2) and supplemented with an excess of sulfo-N-hydroxysuccinimide (NHS, Sigma) and 1-ethyl-3-(3-dimethylaminopropyl) carbodiimide hydrochloride (EDC, Sigma). The mixture was allowed to stir overnight after addition of methoxypolyethylene glycol amine (90 µmol, MW: 2 000, Sigma). The resulting product was subsequently lyophilized after 24 h of dialysis against distilled water (Spectra/Por® Dialysis Membrane MWCO 15 kDa). The structure of PGA-PEG shown in Figure 3 was confirmed by ^{1}H NMR spectroscopy.

2.4 PEGylation of Dextran Nanogels. Nanogels were PEGylated in three different ways. Firstly, methoxypolyethylene glycol 5000 (PEG, Sigma) was added to a 1 mg mL^{-1} nanogel dispersion in order to evaluate the effects of physical adsorption. Secondly, increasing amounts of PGA-PEG were added to a 1 mg mL^{-1} nanogel dispersion to induce PEGylation based on electrostatic interactions. Finally, increasing amounts of N-hydroxysuccinimidyl activated methoxypolyethylene glycol 5000 propionic acid (NHSPEG, Sigma) were added to a 1 mg mL^{-1} nanogel dispersion for minimum 30 minutes to achieve a covalent PEGylation. Aliquots of these samples were diluted and briefly sonicated before measuring the size and zeta potential by DLS.

2.5 Small Interfering RNA (siRNA). Dicer substrate 25/27-mer siRNA targeting EGFP and dicer substrate 25/27-mer negative control (NC-1) were provided by IDT (Leuven, Belgium). Anti-EGFP siRNA: 5'-pACCCUGAAGUUCAUCUGCACCACcg-3', 3'-ACUGGGACUUCAAGUAGACGUGGUGGC-5'. NC-1: 5'- pCGUUAAUCGCGUAUAAUACGCGUat-3', 3'-CAGCAAUUAGCGCAUAUUAUGCGCAUAp-5'.

AlexaFluor 488-labeled 25/27-mer siRNA (AF488-siRNA) targeting EGFP was also provided by IDT. Lyophilized siRNA was dissolved in 30 mM HEPES buffer containing 100 mM potassium acetate (pH 7.5). The solution was incubated for 30 s at 94°C and allowed to cool to room temperature prior to spectrophotometric determination of the concentration. The siRNA was aliquoted and stored at -20 °C before use.

2.6 Ninhydrin Assay. In order to quantitate the reactive primary amines on the nanogels, 1 mL of a 0.25 mg mL^{-1} nanogel dispersion in 1 M acetic acid was incubated with 1 mL ninhydrin/hydrindantin solution for 15 min at 100 °C. Dex-MA based nanogels had to be used because the exposure to high temperatures during this assay causes fast hydrolysis of dex-HEMA nanogels. Samples were left to cool to room temperature and stabilized with 50% v/v ethanol before performing absorption measurements at 570 nm using a UV-1800 UV-VIS Spectrophotometer (Shimadzu, Belgium). All samples were prepared in triplicate and their amine content was calculated using a glycine standard curve.

2.7 Fluorescence Recovery After Photobleaching (FRAP). To assess the nature of the interactions between the dextran nanogels and the siRNA molecules, *micron* sized dextran gel particles (with the same composition as the sized dextran *nano*gels) were prepared as described earlier by our group (Raemdonck et al., 2008a). These dextran microgels were

loaded with AF488-labeled anti-EGFP siRNA (IDT, Leuven, Belgium) in a similar manner to the dextran nanogels used in the transfection experiments (see 2.13). The FRAP experiments were performed on a CLSM (model MRC1024 UV, Bio-Rad, Hemel Hempstead, UK) modified to be able to bleach arbitrary regions (De Geest et al., 2005). All bleaching experiments were performed with the 488-nm line of a 4 W Ar-ion laser (model Stabilite 2017; Spectra-Physics, Darmstadt, Germany). In general, the intensity of the bleaching beam was 1000 to 10 000 times higher than the detection beam. A 10x objective lens (CFI Plan Apochromat; Nikon, Badhoevedorp, The Netherlands) with a numerical aperture (NA) of 0.45 was used.

2.8 Fluorescence Fluctuation Spectroscopy (FFS). A fluorescence fluctuation spectroscopy instrument was used to quantify the percentage of siRNA complexation by the (PEGylated) nanogels (Raemdonck et al., 2009b). FFS monitors fluorescence intensity fluctuations in the excitation volume of a confocal microscope. The fluorescence fluctuations originate from the movement of fluorescent molecules (in this study AF488-siRNA) through a fixed confocal excitation volume. We showed recently that this fluorescence fluctuation profile can be used to calculate the percentage of fluorescently labeled siRNA complexed by carriers such as liposomes and cationic polymers. For more details on this method we refer to the appropriate references (Buyens et al., 2008, Buyens et al., 2009). Typically, for FFS experiments, 25 µL of a non-PEGylated nanogel dispersion (1 mg mL^{-1}) was mixed with 25 µL of an AF488-siRNA solution (2 µM) in RNase free Eppendorf tubes and incubated for 10 min. The nanogels were subsequently PEGylated by adding 25 µL of a PEG 5000 solution (1 mg mL^{-1}), NHS-PEG 5000 solution (1 mg mL^{-1}) or PGA-PEG solution (0.05 mg mL^{-1}) and allowed to react for 30 min. Subsequently, the samples were diluted and transferred to a glass-bottomed 96-well plate (Greiner Bio-one, certified DNase/RNase free). The focal volume of

the FFS-microscope was positioned 50 µm above the bottom of the wells and the fluorescence fluctuations were recorded during a 30 s time interval using the 488nm laser line of a krypton-argon ion laser (BioRad, Cheshire, UK). All samples were prepared in triplicate and every measurement was performed three times. The percentage of siRNA loaded by the nanogels was calculated from the fluorescence fluctuation profile as described earlier by Buyens et al (Buyens et al., 2008, Raemdonck et al., 2009b).

2.9 Cell Lines and Culture Conditions. Cell experiments were conducted on a human hepatoma cell line called HuH-7 and human epithelial carcinoma cells (A431, a kind gift from Dr. Tony Lahoutte, VUB, Belgium). HuH-7 cells stably expressing enhanced green fluorescent protein (HuH-7_EGFP) were generated by transfecting HuH-7 cells with the pEGFP-N2 plasmid (Clontech, Palo Alto, USA). The pDNA was linearized using the restriction enzyme XbaI and transfected by complexation with linear polyethylenimine (PEI) of MW 22 kDa. Transfected cells were incubated in fresh medium for 48 h and then selected with 400 µg mL^{-1} G418 (geneticine, Invitrogen). After two weeks, clones were isolated and expanded. Subsequently, the clones generated were analyzed by confocal laser scanning microscopy (CLSM) and a 100 % EGFP positive clone was selected. All cell lines were grown in Dulbecco's modified Eagle medium (DMEM):F12, supplemented with 2 mM glutamine, 10% fetal bovine serum (FBS) and 100 U mL^{-1} penicillin-streptomycin at 37 °C in a humidified atmosphere containing 5% CO_2.

2.10 Cytotoxicity Assay. The influence of PEGylated and non-PEGylated nanogels on the cell viability was analyzed using the CellTiter-Glo Assay (Promega). HuH-7 cells ($4x10^4$ cells per cm^2) were seeded in 24-well plates and allowed to adhere. After 48 h, the culture medium

was removed and replaced by 200 µL of a nanogel dispersion in OptiMEM. Following 4h of incubation (37 °C, 5% CO_2), nanogels that were not internalized were removed from the cells and replaced with 200 µL of preheated culture medium. The 24-well plates were incubated another 24h at 37 °C before cell viability was analyzed by incubating the plates at room temperature for 30 min and adding 200 µL CellTiter-Glo reagent to each well. After shaking the plate for 2 min (to lyse the cells) and 10 min of incubation at room temperature (to stabilize the luminescence signal), 100 µL from each well was transferred to a white-opaque 96-well plate. Luminescence was measured on a GloMax 96 luminometer with 1 s integration time. Cells treated with OptiMEM alone and cells incubated with phenol (10 mg mL^{-1}) served as negative and positive controls respectively.

2.11 Confocal Laser Scanning Microscopy. Wild type HuH-7 cells (HuH-7_WT) were seeded in sterile glass-bottomed culture dishes (MatTek Corporation, Ashland, MA) at a density of $4x10^4$ cells per cm^2 and allowed to attach overnight. Nanogels loaded with AF488-siRNA in 200 µL OptiMEM were incubated with the cells for 4 h (37 °C, 5% CO_2). Subsequently, the cells were washed with phosphate buffered saline (PBS) and preheated culture medium was added. The intracellular fluorescence distribution was visualized with a Nikon C1si confocal scanning module installed on a motorized Nikon TE2000-E inverted microscope (Nikon Benelux, Brussels, Belgium). Confocal images were captured with a Nikon Plan Apochromat 60x oil immersion objective (numerical aperture 1.4) using a 488-nm laser line for the excitation of AF488-siRNA. A non-confocal diascopic differential interference contrast (DIC) image was collected simultaneously.

2.12 Flow Cytometry. Cellular uptake of nanogels was quantified by flow cytometry. HuH-7_EGFP cells were plated in 24-well plates ($4x10^4$ cells per cm^2) and were allowed to attach for 24 h. Cells were incubated for 4 h with siRNA-loaded nanogels (200 nM AF488-siRNA per well), prepared as described above. Cells equally treated and incubated at 10°C to inhibit endocytosis were used as negative controls. After this incubation period, the cells were washed with PBS and incubated for 7 min with 0.2% (v/v) trypan blue to quench extracellular fluorophores. The cells were washed three times with PBS, trypsinized (100 µL of 0.25% trypsin per well) and diluted with 700 µL cell culture medium. Following centrifugation (7 min, 1100 rpm), the cell pellet was resuspended in 300 µL flow buffer (PBS supplemented with 1% BSA and 0.1% sodium azide) and placed on ice prior to measurement on a Beckman Coulter Cytomics FC500 flow cytometer. Generally, a minimum of $2x10^4$ cells were analyzed in each measurement. Dead cells were discriminated from viable cells by the addition of propidium iodide. The data were analyzed using Beckman Coulter CXP analysis software.

2.13 EGFP Gene Silencing. HuH-7_EGFP cells were plated in 24-well plates ($4x10^4$ cells per cm^2) and were allowed to attach for 24 h. Nanogels were dispersed in HEPES buffer and subsequently loaded (as described above) with either negative control siRNA (NC-1) or EGFP targeting siRNA. Particles were PEGylated by adding NHS-PEG to the nanogels at an NHS-PEG/nanogels weight ratio of 5. After 30 min, the nanogels were diluted with OptiMEM to the desired concentrations before adding 200 µl of the dispersions to each well. After a 4 h incubation period, the nanogel dispersion was replaced by 1 mL of fresh culture medium. All plates were incubated for a further 72 h before EGFP expression was quantified using a Beckman Coulter Cytomics FC500 flow cytometer. All transfections were performed four times and the data were analyzed using Beckman Coulter CXP analysis software.

3. Results and discussion

3.1 Preparation of dex-(HE)MA-*co*-AEMA-*co*-TMAEMA Nanogels. As schematically illustrated in Figure 4, dextran nanogels were prepared by inverse mini-emulsion photopolymerization (Raemdonck et al., 2009b). In this process, a known amount of dex-HEMA (or dex-MA) is dissolved in buffer and supplemented with AEMA, TMAEMA and the photoinitiator. This water phase is added to mineral oil containing the surfactant. After crosslinking, washing, lyophilization and redispersing of the lyophilized nanogels in buffer, a hydrodynamic diameter between 150 and 200 nm and a zeta-potential between 20 and 25 mV were measured by dynamic light scattering (data not shown). As explained in the materials and methods section, the total amount of cationic methacrylates was kept constant at 0.5 mmol. Figure 5 shows the relationship between the percentage of AEMA in the total amount of cationic monomers and the relative amount of primary amines on the nanogels as measured by a ninhydrin assay. The experiment proves that the copolymerization of AEMA is indeed responsible for the introduction of reactive amines in the gels.

3.2 Degradation of dex-HEMA-*co*-AEMA-*co*-TMAEMA Nanogels . We showed recently that dex-HEMA-*co*-TMAEMA nanogels are susceptible to pH dependent degradation due to hydrolysis of the carbonate ester of dex-HEMA (Figure 2) (Raemdonck et al., 2009b). Similar degradation profiles are to be expected for dex-HEMA-*co*-AEMA-*co*-TMAEMA nanogels provided that aminolysis does not occur during the synthesis of the gels. During the process of aminolysis, primary amino groups may react with the carbonate esters of dex-HEMA,

generating amide based linkages which are not susceptible to hydrolysis (Kloeckner et al., 2006). Figure 6 shows however that the degradation kinetics of the dex-HEMA-*co*-AEMA-*co*-TMAEMA ratio 1:4 nanogels is similar to nanogels composed of dex- HEMA-*co*-TMAEMA. It is indeed to be expected that large scale aminolysis does not occur considering the temperatures at which the nanogels are produced. Note in Figure 6 that nanogels containing dex-MA, which lack hydrolyzable carbonate esters indeed do not degrade over time. The slight decrease in light scattering as a function of time can likely be attributed to nonspecific adsorption of the nanogels to the DLS cuvettes. A plausible reason for the faster degradation rate of nanogels composed of higher TMAEMA/AEMA ratios (compare curves 3 and 5 in Figure 6) is the fact that TMAEMA may result in a locally higher presence of hydroxide ions. A higher micro-pH in the vicinity of the quarternary amines of TMAEMA could stimulate base-dependent hydrolysis of the dex-HEMA, thus resulting in a faster degradation of the nanogels.

3.3 Influence of siRNA Complexation on Surface Charge of dex-MA-*co*-AEMA-*co*-TMAEMA Nanogels. It is to be expected that the addition of siRNA duplexes to this type of nanogels will decrease the surface charge of the cationic nanogels (Raemdonck et al., 2009b). Figure 7 displays the change in size and zeta-potential of dex-HEMA-co-AEMA-co-TMAEMA nanogels (initially 180 nm in size with a zeta-potential of 12 mV) upon addition of siRNA to nanogel dispersions with a fixed concentration. As shown in Figure 7, neutralization and aggregation was observed after adding approximately 1 nmol siRNA per mg of nanogels. Further addition of siRNA to the nanogel dispersion resulted in negatively charged particles and a 'restabilization' of the dispersion. Note that such an "overloading" of the nanogels with siRNA is unwanted as negatively charged nanogels are taken up less efficiently by cells (data

not shown). Also note that the initial ζ-potential of the nanogels is an important parameter for the loading capacity of the nanogels. In the continuation of this paper, dex-HEMA-co-AEMA-co-TMAEMA nanogels with an initial ζ-potential of more than 20 mV were used to ensure stable dispersions with a sufficiently high surface charge after siRNA loading.

3.4 PEGylation of dex-MA-*co*-AEMA-*co*-TMAEMA Nanogels. Shielding of nanogels with polyethylene glycol could theoretically be achieved in various ways. The most straightforward way to equip nanogels with a PEG coating would be the physical adsorption of PEG to the nanogel surface. It is however predictable that this form of PEGylation will not be stable in complex media like blood due to the fairly low interaction strength between PEG and the gels resulting in an inadequate protection against competing serum proteins. Coupling of PEG to the nanogels through electrostatic interactions could be another suitable approach for PEGylation. For this reason, methoxypolyethylene glycol amine was grafted on poly-L-glutamic acid (PGA-PEG; Figure 3), using a PEG:carboxylic acid ratio of 1:5, in an attempt to cover the cationic nanogels with these negatively charged polymers. As the interactions between PGA-PEG and the nanogels surface is based on multiple electrostatic interactions, this type of PEGylated nanogels might be able to withstand the relatively harsh conditions *in vivo*. A final approach for PEGylating nanogels is the covalent coupling of PEG. As commercially available N-hydroxysuccinimidyl activated methoxypolyethylene glycol 5000 propionic acid (NHS-PEG) can spontaneously react with primary amines, nanogels containing aminoethyl methacrylate were prepared in order to provide the nanogels with reactive amines. Previously designed nanogels did not contain any chemical groups for a mild reaction with activated PEG molecules.

To confirm the interaction between the PEG moieties and the nanogels, the zeta potential and the amount of residual reactive amines on the nanogels after PEGylation were measured (Figure 8). For these experiments, non-degradable nanogels based on dex-MA were used as degradation of the gels during the assays was undesired. As shown in Figure 8A, simple PEG did not alter the positive zeta potential of nanogels significantly while adding increasing amounts of NHS-PEG and PGA-PEG resulted in neutral and negatively charged particles respectively. In addition, incubation of increasing amounts of NHS-PEG lead to a concentration dependent decrease of reactive amine groups on the nanogels (Figure 8B). The use of mere PEG did, as expected, not decrease the amount of reactive amines.

3.5 PEGylation of siRNA loaded dex-MA-*co*-AEMA-*co*-TMAEMA Nanogels. As described in the materials and methods section and as discussed above under 2.4, the cationic nanogels were loaded with siRNA before PEGylation. As the availability of reactive amine groups on the nanogel surface is probably crucial for a successful PEGylation with NHS-PEG, one could speculate that loading the nanogels with siRNA before PEGylation might hamper the coupling reaction by occlusion of the reactive groups. For this reason, we investigated the decrease in reactive amines upon PEGylation of nanogels already loaded with siRNA. A ninhydrin assay was performed on the nanogels loaded with 2 nmol siRNA per mg nanogels. The two bars on the left in Figure 9 show the same normalized amount of reactive amines in non-PEGylated nanogels with or without siRNA. Furthermore, incubation with NHS-PEG causes a similar decrease in the normalized amount of reactive amines on both loaded and unloaded nanogels. This allows us to conclude that preloading of nanogels with siRNA does not interfere with the covalent coupling of NHS-PEG.

3.6 Quantification of siRNA Complexation by non-PEGylated and PEGylated dex-HEMA-*co*-AEMA-*co*-TMAEMA nanogels. The siRNA complexation efficiency of dex-HEMA-co-AEMA-co-TMAEMA nanogels was determined by fluorescence fluctuation spectroscopy (FFS). Details on how FFS enables quantification of the complexation of nucleic acids by carriers can be found elsewhere [(Buyens et al., 2008, Raemdonck et al., 2009b)]. Data presented in Figure 10 indicates a loading efficiency of more than 80% for both dex-HEMA-co-TMAEMA and dex-HEMA-co-AEMA-co-TMAEMA nanogels. The slight difference between the two types of nanogels can likely be explained by a small difference in ζ-potential. Furthermore, Figure 10 shows that addition of PEG or covalent PEGylation with NHS-PEG did not cause the release of siRNA from the nanogels. PEGylation via PGA-PEG caused however a complete dissociation of siRNA from the nanogels which can be attributed to the highly negatively charged polyglutamic acid moieties which compete with siRNA for binding to the cationic groups in the nanogels. PEGylation of the nanogels via PGA-PEG is thus not practical which makes covalent PEGylation the preferred method.

3.7 Assessing the Nature of the Interactions between the dex-HEMA-*co*-AEMA-*co*-TMAEMA Matrix and the siRNA Molecules by FRAP. Fluorescence recovery after photobleaching (FRAP) is typically used to screen the mobility of fluorescent molecules in micrometer sized areas (Braeckmans et al., 2003). A FRAP experiment involves three distinct steps, namely registration of the fluorescence before photobleaching in a well defined area of the sample; fast photobleaching within the defined area using a high power laser beam and subsequent imaging of the fluorescence recovery in the bleached area arising from the diffusional exchange between photobleached molecules and intact ones from the immediate surroundings. It is then possible to extract the diffusion coefficient and the percentage of

immobilized fluorescent molecules in the sample by fitting the experimental fluorescence recovery curve to a suitable mathematical FRAP model (Mazza et al., 2008, Braeckmans et al., 2003).

Figure 11 shows the recovery of fluorescence after bleaching small regions in a dex-HEMA-co-AEMA-co-TMAEMA gel loaded with fluorescent AF488-siRNA. The FRAP results indicate that all (96 %) siRNA molecules are mobile in the dex-HEMA-co-AEMA-co-TMAEMA matrix with an average diffusion coefficient of 0.033 ±0.007 $\mu m^2 s^{-1}$. As the diffusion coefficient of freely diffusing siRNA in buffer is thousands of times faster (as measured by FFS) one can hypothesize that the negatively charged siRNA molecules are still mobile but trapped through continuous interactions with the numerous cationic charges in the gel network.

3.8 Cytotoxicity of non-PEGylated and PEGylated dex-HEMA-*co*-AEMA-*co*-TMAEMA nanogels. Safety and toxicity are without doubt important aspects in the development of siRNA delivery systems. For this reason, acute cytotoxicity of both non-PEGylated and PEGylated dex-HEMA-*co*-AEMA-*co*-TMAEMA nanogels was assessed on human hepatoma cells (HuH-7) by quantification of intracellular adenosine triphosphate (ATP) levels 24 h after applying the nanogels on the cells. Figure 12 shows that the nanogels are well tolerated and that PEGylated nanogels can be used in much higher concentrations then non-PEGylated nanogels. This is likely due to the fact that, compared to the non-PEGylated nanogels, the PEGylated nanogels have less primary amines and are taken up less efficiently by the cells.

3.9 Cellular Uptake of non-PEGylated and PEGylated dex-HEMA-*co*-AEMA-*co*-TMAEMA Nanogels. To assess the influence of PEGylation on the binding of the nanogels to the cellular membrane and the subsequent cellular uptake, flow cytometry and confocal laser

scanning microscopy were used. Results obtained by flow cytometry after 4 h of incubation with either non-PEGylated or PEGylated nanogels loaded with AF488-siRNA are shown in Figure 13. Although the percentage of cells that have taken up nanogels is high and similar for both non-PEGylated and PEGylated nanogels (Figure 13A), the mean fluorescence intensity per cell (Figure 13B) is approximately halved when the nanogels are PEGylated. As non-PEGylated and PEGylated nanogels show a similar siRNA loading efficiency (based on Figure 10), we can conclude that the lower fluorescence intensity per cell in Figure 13B is due to less particles present in the cells. Indeed, interaction with the negatively charged cell membrane and subsequent internalization of the cationic nanogels is probably impaired by PEGylation, causing a less efficient uptake. Although the amount of particles taken up by A431 and HuH-7 is different, PEGylation of the nanogels had a similar effect in both cell lines. Note that all samples were treated with 0.2% trypan blue to exclude measurement of non-internalized nanogels.

The uptake of dex-HEMA-*co*-AEMA-co-TMAEMA nanogels by cells was additionally confirmed by confocal laser scanning microscopy (CLSM). Figure 14 shows that both non-PEGylated and PEGylated nanogels are located intracellularly after 4 h of incubation. All together, these results indicate that, despite a lower ζ-potential, the cellular uptake of PEGylated siRNA loaded nanogels still occurs quite efficiently and is cell type dependent.

3.10 EGFP Gene Silencing by dex-HEMA-*co*-AEMA-*co*-TMAEMA Nanogels in HuH-7_EGFP Hepatoma Cells. The RNAi gene-silencing potential of both non-PEGylated and PEGylated nanogels in HuH-7_EGFP cells was compared. As demonstrated in Figure 15, EGFP silencing clearly occurs, the extent of EGFP silencing depending on the concentration of nanogels

applied. Though the number of PEGylated nanogels taken up per cell is lower when compared to the non-PEGylated nanogels (Figure 13), no differences in silencing efficiency were noticed between non-PEGylated and PEGylated nanogels. This is likely due to the fact that only a small fraction of the siRNA delivered to the cells is necessary for the observed down regulation of the EGFP.

Conclusion

This paper shows that PEGylation of cationic dextran based nanogels through simple physical adsorption of PEG does not result in the shielding of the nanogel surface charge. Exposing the nanogels to PGA-PEG resulted in successful coating but a complete release of encapsulated siRNA. Successful PEGylation of cationic dextran nanogels was obtained by covalent attachment of NHS-PEG to the reactive amine groups of the nanogels. We additionally showed that dex-(HE)-MA-*co*-AEMA-*co*-TMAEMA nanogels retained their high loading efficiency of siRNA after PEGylation. Using fluorescence recovery after photobleaching, we were able to show that the diffusion of the negatively charged siRNA molecules inside the gels occurs very slowly and that the siRNA is probably trapped by the cationic charges in the nanogels. Furthermore, siRNA loaded PEGylated dex-(HE)MA-*co*-AEMA-co-TMAEMA nanogels were able to successfully down regulate EGFP without causing severe toxicity in a HuH-7_EGFP cell line. Our future research will focus on the introduction of ligands for active targeting of these nanogels to specific cell types.

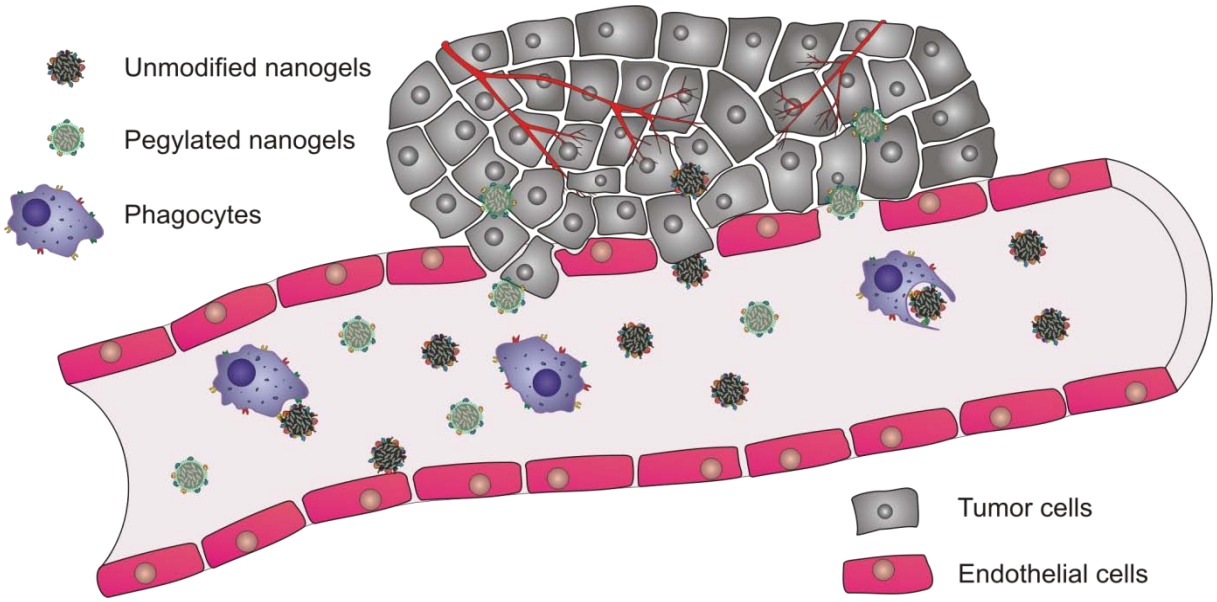

Figure 1. Schematic representation of the clearance of non-PEGylated nanogels by phagocytes in the bloodstream; PEGylation of nanogels should prolong their circulation and thus prolong the time available for extravasation into tumor tissues (Maeda et al., 1999, Ogris and Wagner, 2002). Capillaries in these tissues are often considered leaky due to defects in the endothelium wall which further facilitates the extravasation into the tumor.

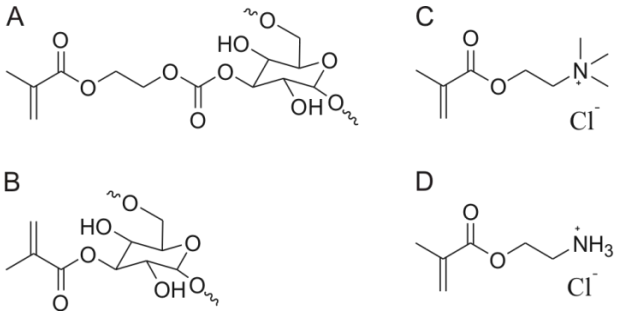

Figure 2. Chemical structure of (A) dextran hydroxyethyl methacrylate (dex-HEMA), (B) dextran methacrylate (dex-MA), (C) [2-(methacryloyl)ethyl]trimethylammonium chloride (TMAEMA) and (D) aminoethyl methacrylate hydrochloride (AEMA). For dex-MA and dex-HEMA a degree of substitution (D.S., i.e. the number of HEMA or MA groups per 100 glucose units) of respectively 5.2 and 5.9 was used.

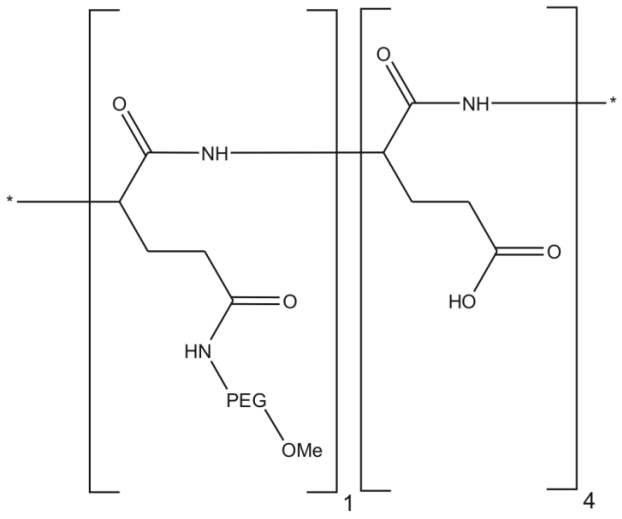

Figure 3. Chemical structure of methoxypolyethylene glycol grafted poly-L-glutamic acid (PGA-PEG).

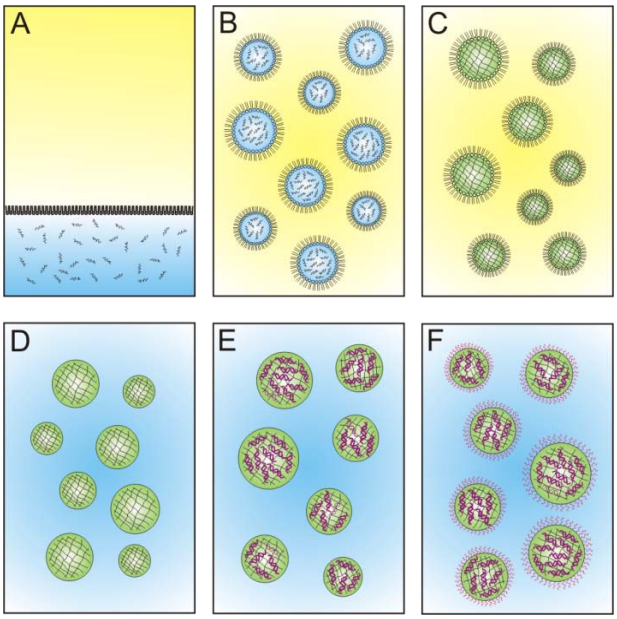

Figure 4. The general procedure for making PEGylated nanogels loaded with siRNA: (A) Two-phase system containing mineral oil with an oil-soluble surfactant (upper phase) and HEPES buffer containing dex-(HE)MA, AEMA, TMAEMA and a photoinitiator (lower phase). (B) Mini-emulsion after sonication. (C) Nanogel formation through UV induced crosslinking. (D) Washing and lyophilization of the nanogels. (E) Nanogel redispersal and loading by incubation with an siRNA solution. (F) PEGylation of the nanogels.

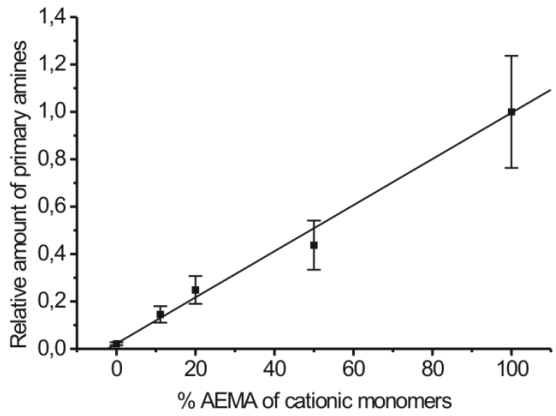

Figure 5. The relative number of primary amines in the dex-MA-*co*-AEMA-*co*-TMAEMA nanogels is proportional to the amount of AEMA used in the synthesis of the nanogels. Nanogel samples were prepared in triplicate and a total amount of 5 mmol of cationic methacrylates/100 mg dex-MA was used.

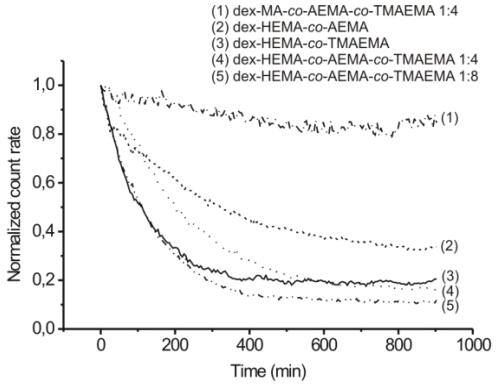

Figure 6. Degradation at 37°C of dex-(HE)MA based nanogels (D.S. 5.2) composed of different ratios of AEMA/TMAEMA. A total amount of 5 mmol cationic methacrylates per 100 mg dex-(HE)MA was used. The light scattered by the nanogel dispersions was measured and the data were normalized to enable comparison. Non-degradable dex-MA-*co*-AEMA-*co*-TMAEMA 1:4 nanogels were used as a negative control.

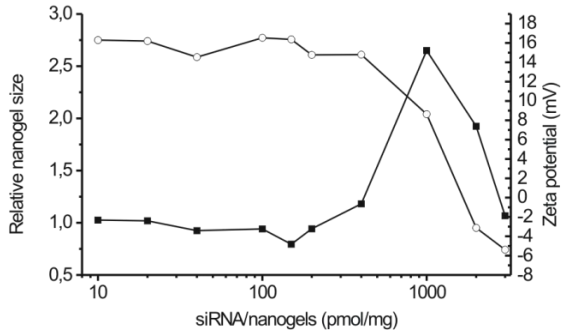

Figure 7. Relative size (■) and zeta-potential (○) of dex-HEMA-*co*-AEMA-*co*-TMAEMA nanogels (125 µg mL^{-1}) after titration with siRNA. Measurements were performed in HEPES buffer at 25°C.

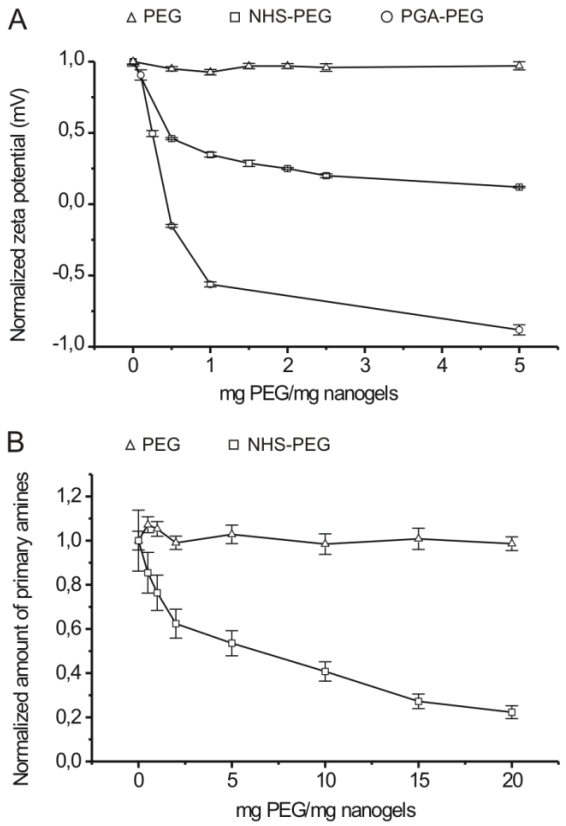

Figure 8. (A) Normalized ζ-potential of dex-MA-*co*-AEMA-*co*-TMAEMA 1:4 nanogels after 30 min incubation with PEG, NHS-PEG and PGA-PEG respectively. (B) Normalized amount of primary amines, as measured by a ninhydrin assay, after addition of respectively PEG or NHS-PEG to dex-MA-*co*-AEMA-*co*-TMAEMA nanogels 1:4. Samples were prepared in triplicate.

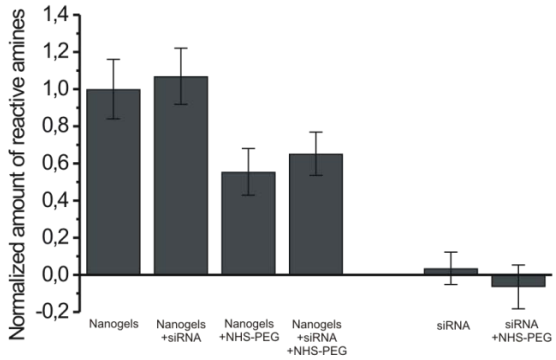

Figure 9. Influence of loading dex-MA-*co*-AEMA-*co*-TMAEMA 1:4 nanogels with siRNA (2000 pmol siRNA/mg nanogels) on the covalent PEGylation with NHS-PEG. 5 mg of NHS-PEG per mg nanogels was used throughout the experiment. All samples were prepared in triplicate (n=3).

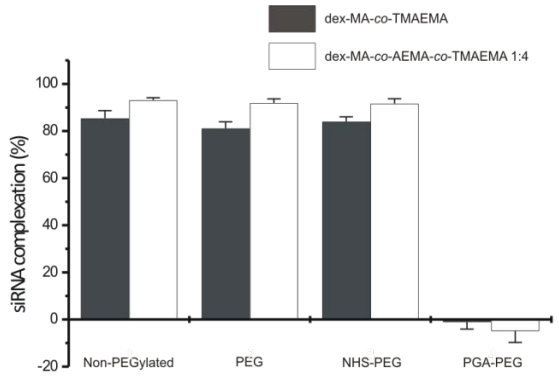

Figure 10. AF488-siRNA complexation by cationic dex-HEMA nanogels measured by FFS. Samples were prepared in triplicate and measured 1 h after PEGylation of the nanogels.

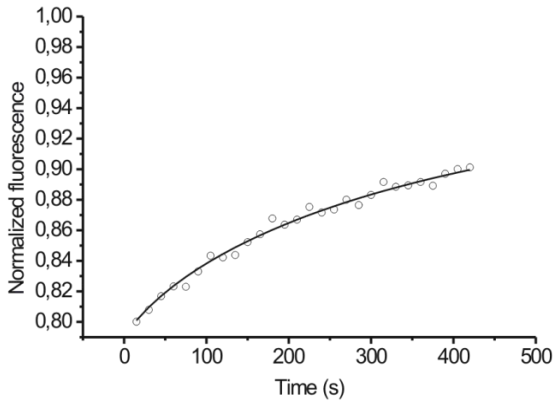

Figure 11. Fluorescence recovery after photobleaching in dex-MA-*co*-AEMA-*co*-TMAEMA 1:4 gels loaded with AF488-siRNA. The average diffusion coefficient of the AF488-siRNA molecules in the dex-MA-*co*-AEMA-*co*-TMAEMA gel matrix was 0.033 ± 0.007 $\mu m^2 s^{-1}$. The mobile fraction of AF488-siRNA molecules was 96 ± 4 %.

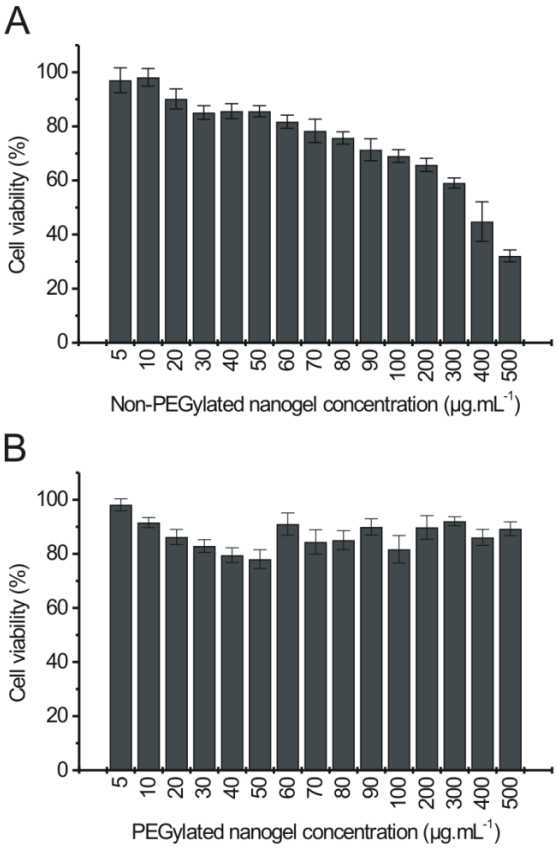

Figure 12. Cell viability of HuH-7 hepatoma cells, incubated for 4 h with (A) non-PEGylated dex-HEMA-*co*-AEMA-*co*-TMAEMA nanogels and (B) PEGylated dex-HEMA-*co*-AEMA-*co*-TMAEMA nanogels. The intracellular ATP-levels were determined 24 h after the nanogels were removed from the cells. ATP-levels of untreated cells were set as 100% and all data are shown as mean ±SD (n=4).

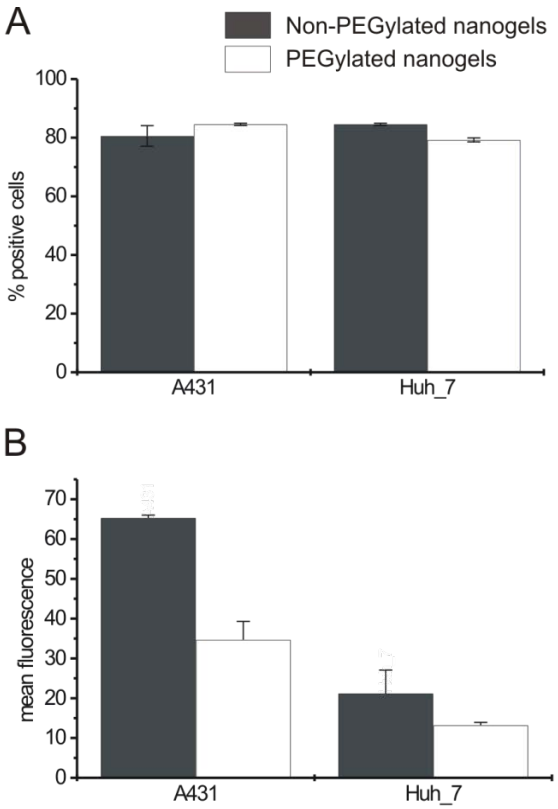

Figure 13. Flow cytometry results obtained after treating HuH-7 cells with AF488-siRNA loaded dex-HEMA-*co*-AEMA-*co*-TMAEMA nanogels. (A) depicts the percentage of positive cells in the total population. (B) shows the mean fluorescence per cell. All samples were prepared in triplicate and incubated with trypan blue before flow cytometry measurements.

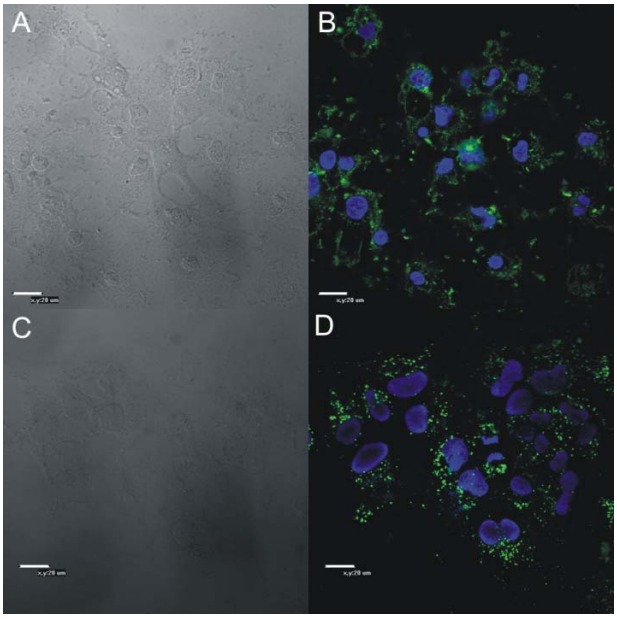

Figure 14. Confocal images of the intracellular distribution of AF488-siRNA (green) loaded dex-HEMA-*co*-AEMA-*co*-TMAEMA 1:4 in HuH-7 hepatoma cells. (A) Nonconfocal DIC image non-PEGylated nanogels, (B) fluorescence image non-PEGylated AF488-siRNA nanogels, (C) Nonconfocal DIC image PEGylated nanogels, (D) fluorescence image PEGylated AF488-siRNA nanogels. siRNA loaded nanogels (10 µg mL $^{-1}$, 200 pmol mL^{-1} siRNA) were incubated for 4 h, followed by a 24 h chase with cell culture medium. The samples were fixed with paraformaldehyde and extracellular fluorophores were quenched with trypan blue. Nuclei were stained with DAPI (blue). The scale bar represents 20 µm.

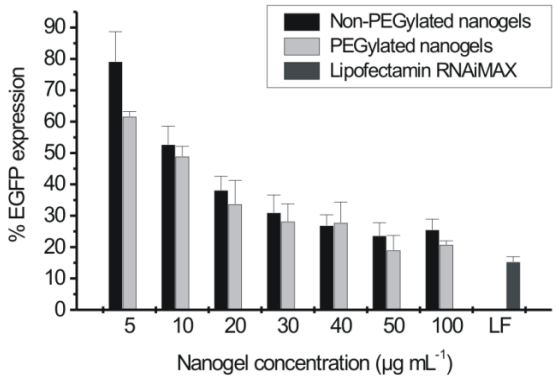

Figure 15. EGFP gene silencing by both non-PEGylated and PEGylated dex-HEMA-*co*-AEMA-*co*-TMAEMA 1:4 nanogels in HuH-7_EGFP cells. Increasing concentrations of nanogels were applied (4h incubation) and Lipofectamin RNAiMAX was used as a positive control. The used amount of siRNA per well was 50 pmol and the EGFP expression of cells treated with nanogels loaded with mock NC-1 siRNA was set as 100%.

BAZILE, D., PRUDHOMME, C., BASSOULLET, M. T., MARLARD, M., SPENLEHAUER, G. & VEILLARD, M. 1995. STEALTH ME.PEG-PLA NANOPARTICLES AVOID UPTAKE BY THE MONONUCLEAR PHAGOCYTES SYSTEM. *Journal of Pharmaceutical Sciences,* 84**,** 493-498.

BRAASCH, D. A., PAROO, Z., CONSTANTINESCU, A., REN, G., OZ, O. K., MASON, R. P. & COREY, D. R. 2004. Biodistribution of phosphodiester and phosphorothioate siRNA. *Bioorganic & Medicinal Chemistry Letters,* 14**,** 1139-1143.

BRAECKMANS, K., PEETERS, L., SANDERS, N. N., DE SMEDT, S. C. & DEMEESTER, J. 2003. Three-dimensional fluorescence recovery after photobleaching with the confocal scanning laser microscope. *Biophysical Journal,* 85**,** 2240-2252.

BUYENS, K., DEMEESTER, J., DE SMEDT, S. C. & SANDERS, N. N. 2009. Elucidating the Encapsulation of Short Interfering RNA in PEGylated Cationic Liposomes. *Langmuir,* 25**,** 4886-4891.

BUYENS, K., LUCAS, B., RAEMDONCK, K., BRAECKMANS, K., VERCAMMEN, J., HENDRIX, J., ENGELBORGHS, Y., DE SMEDT, S. C. & SANDERS, N. N. 2008. A fast and sensitive method for measuring the integrity of siRNA-carrier complexes in full human serum. *Journal of Controlled Release,* 126**,** 67-76.

DE GEEST, B. G., DEJUGNAT, C., SUKHORUKOV, G. B., BRAECKMANS, K., DE SMEDT, S. C. & DEMEESTER, J. 2005. Self-rupturing microcapsules. *Advanced Materials,* 17**,** 2357-+.

ELBASHIR, S. M., HARBORTH, J., LENDECKEL, W., YALCIN, A., WEBER, K. & TUSCHL, T. 2001. Duplexes of 21-nucleotide RNAs mediate RNA interference in cultured mammalian cells. *Nature,* 411**,** 494-498.

FIRE, A., XU, S. Q., MONTGOMERY, M. K., KOSTAS, S. A., DRIVER, S. E. & MELLO, C. C. 1998. Potent and specific genetic interference by double-stranded RNA in Caenorhabditis elegans. *Nature,* 391**,** 806-811.

GARCIA-CHAUMONT, C., SEKSEK, O., GRZYBOWSKA, J., BOROWSKI, E. & BOLARD, J. Year. Delivery systems for antisense oligonucleotides. *In:* 7th Symposium of the European-Society-for-Study-of-Purine-and-Pyrimidine-Metabolism-in-Man (ESSPPMM), Sep 15-19 1999 Gdansk, Poland. Pergamon-Elsevier Science Ltd, 255-277.

GRIMM, D. 2009. Small silencing RNAs: State-of-the-art. *Advanced Drug Delivery Reviews,* 61**,** 672-703.

HARPER, G. R., DAVIES, M. C., DAVIS, S. S., TADROS, T. F., TAYLOR, D. C., IRVING, M. P. & WATERS, J. A. 1991. STERIC STABILIZATION OF MICROSPHERES WITH GRAFTED POLYETHYLENE OXIDE REDUCES PHAGOCYTOSIS BY RAT KUPFFER CELLS-INVITRO. *Biomaterials,* 12**,** 695-704.

HOBBS, S. K., MONSKY, W. L., YUAN, F., ROBERTS, W. G., GRIFFITH, L., TORCHILIN, V. P. & JAIN, R. K. 1998. Regulation of transport pathways in tumor vessels: role of tumor type and microenvironment. *Proc Natl Acad Sci U S A,* 95**,** 4607-12.

HOWARD, M. D., JAY, M., DZIUBLAL, T. D. & LU, X. L. 2008. PEGylation of nanocarrier drug delivery systems: State of the art. *Journal of Biomedical Nanotechnology,* 4**,** 133-148.

KLOECKNER, J., BRUZZANO, S., OGRIS, M. & WAGNER, E. 2006. Gene carriers based on hexanediol diacrylate linked oligoethylenimine: Effect of chemical structure of polymer on biological properties. *Bioconjugate Chemistry,* 17**,** 1339-1345.

MAEDA, H., WU, J., SAWA, T., MATSUMURA, Y. & HORI, K. Year. Tumor vascular permeability and the EPR effect in macromolecular therapeutics: a review. *In:* 9th International Symposium on Recent Advances in Drug Delivery Systems, Feb 22-25 1999 Salt Lake City, Utah. Elsevier Science Bv, 271-284.

MAZZA, D., BRAECKMANS, K., CELLA, F., TESTA, I., VERCAUTEREN, D., DEMEESTER, J., DE SMEDT, S. S. & DIASPRO, A. 2008. A new FRAP/FRAPa method for three-dimensional diffusion measurements based on multiphoton excitation microscopy. *Biophysical Journal,* 95**,** 3457-3469.

MOGHIMI, S. M. & BONNEMAIN, B. 1999. Subcutaneous and intravenous delivery of diagnostic agents to the lymphatic system: applications in lymphoscintigraphy and indirect lymphography. *Advanced Drug Delivery Reviews,* 37**,** 295-312.

MOGHIMI, S. M., HEDEMAN, H., MUIR, I. S., ILLUM, L. & DAVIS, S. S. 1993. AN INVESTIGATION OF THE FILTRATION CAPACITY AND THE FATE OF LARGE FILTERED STERICALLY-STABILIZED MICROSPHERES IN RAT SPLEEN. *Biochimica Et Biophysica Acta,* 1157**,** 233-240.

MOGHIMI, S. M. & PATEL, H. M. 1998. Serum-mediated recognition of liposomes by phagocytic cells of the reticuloendothelial system - The concept of tissue specificity. *Advanced Drug Delivery Reviews,* 32**,** 45-60.

MOGHIMI, S. M. & SZEBENI, J. 2003. Stealth liposomes and long circulating nanoparticles: critical issues in pharmacokinetics, opsonization and protein-binding properties. *Progress in Lipid Research,* 42**,** 463-478.

NOVOBRANTSEVA, T. I., AKINC, A., BORODOVSKY, A. & DE FOUGEROLLES, A. 2008. Delivering silence: Advancements in developing siRNA therapeutics. *Current Opinion in Drug Discovery & Development,* 11**,** 217-224.

OGRIS, M. & WAGNER, E. 2002. Targeting tumors with non-viral gene delivery systems. *Drug Discovery Today,* 7**,** 479-485.

OWENS, D. E. & PEPPAS, N. A. 2006. Opsonization, biodistribution, and pharmacokinetics of polymeric nanoparticles. *International Journal of Pharmaceutics,* 307**,** 93-102.

PACK, D. W., HOFFMAN, A. S., PUN, S. & STAYTON, P. S. 2005. Design and development of polymers for gene delivery. *Nature Reviews Drug Discovery,* 4**,** 581-593.

RAEMDONCK, K., DEMEESTER, J. & DE SMEDT, S. 2009a. Advanced nanogel engineering for drug delivery. *Soft Matter,* 5**,** 707-715.

RAEMDONCK, K., NAEYE, B., BUYENS, K., VANDENBROUCKE, R. E., HOGSET, A., DEMEESTER, J. & DE SMEDT, S. C. 2009b. Biodegradable Dextran Nanogels for RNA Interference: Focusing on Endosomal Escape and Intracellular siRNA Delivery. *Advanced Functional Materials,* 19**,** 1406-1415.

RAEMDONCK, K., VAN THIENEN, T. G., VANDENBROUCKE, R. E., SANDERS, N. N., DEMEESTER, J. & DE SMEDT, S. C. 2008a. Dextran microgels for time-controlled delivery of siRNA. *Advanced Functional Materials,* 18**,** 993-1001.

RAEMDONCK, K., VANDENBROUCKE, R. E., DEMEESTER, J., SANDERS, N. N. & DE SMEDT, S. C. 2008b. Maintaining the silence: reflections on long-term RNAi. *Drug Discovery Today,* 13**,** 917-931.

TAKAKURA, Y., NISHIKAWA, M., YAMASHITA, F. & HASHIDA, M. 2002. Influence of physicochemical properties on pharmacokinetics of non-viral vectors for gene delivery. *Journal of Drug Targeting,* 10**,** 99-104.

VAN DE WATER, F. M., BOERMAN, O. C., WOUTERSE, A. C., PETERS, J. G. P., RUSSEL, F. G. M. & MASEREEUW, R. 2006. Intravenously administered short interfering RNA accumulates in the kidney and selectively suppresses gene function in renal proximal tubules. *Drug Metabolism and Disposition,* 34**,** 1393-1397.

VAN THIENEN, T. G., LUCAS, B., FLESCH, F. M., VAN NOSTRUM, C. F., DEMEESTER, J. & DE SMEDT, S. C. 2005. On the synthesis and characterization of biodegradable dextran nanogels with tunable degradation properties. *Macromolecules,* 38**,** 8503-8511.

VANDIJKWOLTHUIS, W. N. E., TSANG, S. K. Y., KETTENESVANDENBOSCH, J. J. & HENNINK, W. E. 1997. A new class of polymerizable dextrans with hydrolyzable groups: hydroxyethyl methacrylated dextran with and without oligolactate spacer. *Polymer,* 38**,** 6235-6242.

WHITEHEAD, K. A., LANGER, R. & ANDERSON, D. G. 2009. Knocking down barriers: advances in siRNA delivery. *Nature Reviews Drug Discovery,* 8**,** 129-138.

WISSE, E., JACOBS, F., TOPAL, B., FREDERIK, P. & DE GEEST, B. 2008. The size of endothelial fenestrae in human liver sinusoids: implications for hepatocyte-directed gene transfer. *Gene Therapy,* 15**,** 1193-1199.